Multi-Mode Hybrid Antennas Using Liquid Dielectric Resonator and Magneto-Electric Dipole

Chaoyun Song, *Member, IEEE*, Elliot L. Bennett, Jianliang Xiao, and Yi Huang, *Senior Member, IEEE*

Abstract—This paper presents a new type of hybrid antenna that combines the multi-resonant modes produced by a liquid dielectric resonator antenna (DRA) and a magnetoelectric (ME) dipole. Such a combination could not be easily realized by using conventional solid dielectrics due to fabrication and air-gap problems. An aperture-fed ME dipole for 4.1 – 5.3 GHz is firstly designed using a standard structure and a relatively small dimension. Then, a hybrid antenna is built by loading the ME-dipole with an aperture-fed cylindrical liquid DRA. Without increasing the antenna size and/or modifying the ME-dipole structure significantly, the hybrid antenna has realized a much wider bandwidth from 2.45 to 5.3 GHz after loading the liquid material. Moreover, it is found that the resonances of the ME-dipole are not simply shifted to lower frequencies after using the dielectric loading, it has strategically combined the multiple resonances of the electric dipole, magnetic dipole, DRA and feeding slot. The mode combination principle and design guideline have been presented. As an example, a prototype of the proposed hybrid antenna has achieved a 73.5% fractional bandwidth with an electrical size of $0.66 \times 0.66 \times 0.16 \lambda_0^3$ at the centre frequency (3.88 GHz), over 5 dBi (up to 7 dBi) broadside gain, total efficiency > 80% and beam-width around 80 – 120° across the frequency band. The proposed hybrid antenna has advantages in terms of wide bandwidth, smaller size and simple structure compared with other ME-dipoles and traditional wideband antennas. The idea of this antenna design could be extended to other ME-dipole and DRA structures.

Index Terms— Complementary antennas, dielectric resonator antenna (DRA), hybrid antennas, liquid antennas, magneto-electric (ME) dipole antennas, wideband antennas.

I. INTRODUCTION

MODERN wireless communication systems often require advanced antenna technologies which can achieve stable performance in terms of gain, beam-width, and radiation pattern over a wide frequency band including the 2G/3G/4G and future 5G communication spectrums [1]. Conventional wideband antennas can only maintain the stable performance in a certain frequency range since their radiation pattern may vary significantly when the frequency goes high. In 2006, Luk and Wong at the City University of Hong Kong firstly proposed a new type of complementary antenna through the combination of a dipole and a shorted patch antenna, which was designated as the magneto-electric (ME) dipole [2]. Since then, many research activities have been productively conducted in this area [3]-[7]. It has been demonstrated that the ME dipole could exhibit a wide impedance bandwidth, a stable gain, and a stable broadside radiation pattern with low cross-polarization and back radiation levels over the operating frequencies. Therefore, the ME dipole antenna becomes particularly suitable for mobile base-station applications.

One unneglectable drawback of the ME dipole is that the antenna is typically of high profile (e.g., ground plane > $1\lambda_0$ and antenna height $\approx 0.25 \lambda_0$) if the desired bandwidth > 70% and front-to-back-ratio > 15 dB. Some efforts have been made in order to reduce the antenna height of the ME-dipole. In [8], a low-profile design has been achieved through the folding of the shorted patch, consequently achieving a reduced height of $0.169 \lambda_0$. Moreover, an obtuse-triangular structure has been proposed to replace the magnetic dipole, which eventually reduced the antenna height down to $0.097\lambda_0$ [9]. However, the overall fabrication complexity and cost of these antennas are significantly increased if comparing with the typical ones with a simple structure. On the other hand, metamaterial loading [10] and dielectric loading [11] techniques have been reported with the aim to reduce the overall size of the ME dipole. But, it was found that the ME dipole can only be partially loaded due to its complex 3D structure, thus the miniaturization of the antenna is limited, resulting in an overall antenna size still > $1 \lambda_0$[10].

A dielectric material-based ME dipole is reported in [12] where the overall dimension is around $1.15 \times 1.15 \times 0.21 \lambda_0^3$. But this design was based on solid materials while the realized bandwidth was relatively narrow (11.4%). Apart from the solid dielectrics, recent work on using liquid materials to make dielectric resonator antennas (DRAs) has attracted a significant attention [13]-[17]. The liquid DRA has advantages in such as avoiding air-gap problem in the feeding structure and improving the flexibility in fabrication, design and operation. Therefore, the liquid dielectrics could be more suitable for
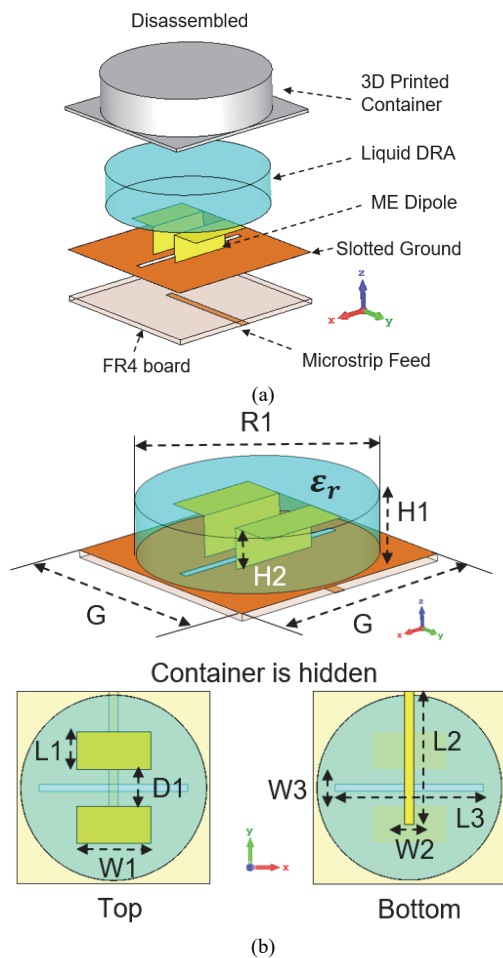
Fig. 1. (a) Disassembled view of the proposed liquid DR and ME dipole antenna. (b) Top, bottom, and perspective views of the antenna.

TABLE I
GEOMETRIC PARAMETERS OF THE PROPOSED ANTENNA

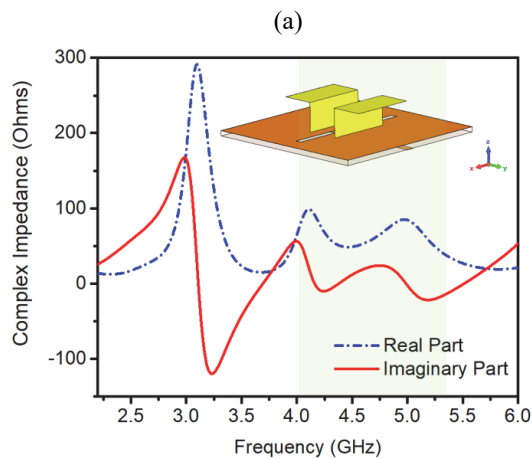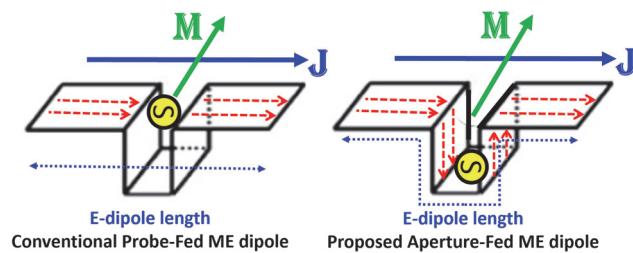| Parameter	R1	H1	G	L1	W1	D1
Value (unit: mm)	50	12	52	10	20	10
Parameter	L2	W2	L3	W3	H2	ε_r
Value (unit: mm)	36	2.5	40	2	9	3.2*

Fig. 2. (a) Comparison between the conventional probe-fed ME-dipole and the proposed aperture-fed ME-dipole in terms of the signal excitation location and electric dipole length. Simulated (b) input impedance and (c) S_{11} of the ME-dipole antenna without loading the liquid DRA. The 3D radiation patterns at 4.3 GHz and 5 GHz are shown as well.

dielectric loading since the antenna can be fully "immersed" into the liquid [18]. Most reported liquid DRAs were made of water and organic solvents. Unfortunately, they have various limitations. For example, water will freeze below 0°C while the solvents could be flammable and evaporate easily. Different from these well-known liquids, our research team at the University of Liverpool has recently explored a range of low-loss dielectric ionic liquids with very stable material properties and an extremely wide liquid range in terms of melting and decomposition temperatures, which are very suitable for practical antenna and RF/microwave devices [18]-[21].

In this paper, we present a new type of hybrid liquid DRA and ME dipole antenna with a wide bandwidth as well as a smaller dimension. As a starting point, a small-sized, aperture-fed ME-dipole antenna with a fractional bandwidth of 25.5% and an electrical size of $0.81\lambda_0 \times 0.81\lambda_0 \times 0.17\lambda_0$ (λ_0 represents the wavelength at center frequency) is firstly designed. Then, a

hybrid antenna is built by loading the ME-dipole with an aperture-fed cylindrical liquid DRA. Consequently, the realized bandwidth is increased from 25.5% (ME-dipole only) to 73.5% (hybrid antenna). In addition, the physical size of the antenna is unchanged throughout the design process, around $52 \times 52 \times 13.6$ mm³. But the lowest resonant frequency has been reduced from 4.1 GHz (ME-dipole only) to 2.45 GHz (hybrid antenna), therefore reducing the antenna size. More importantly, we have found that the resonances of the proposed hybrid antenna are not simply shifted by the dielectric loading effect. Instead, the hybrid antenna has effectively combined four different resonant modes over the bandwidth, namely, the electric dipole mode, magnetic dipole mode, DRA mode and slot mode. New theory on the multiple mode combination and design guideline of the
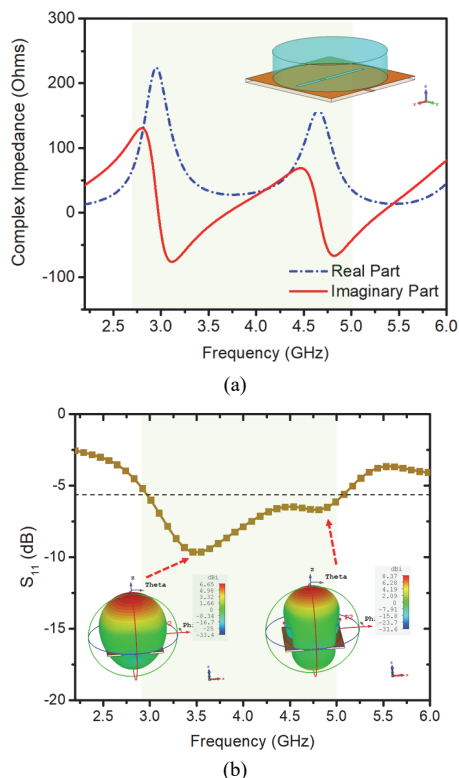
(a)

(b)

Fig. 3. Simulated (a) input impedance and (b) S_{11} of the cylinder DRA without loading the ME dipole. The 3D radiation patterns at 3.5 GHz and 5 GHz are shown as well.
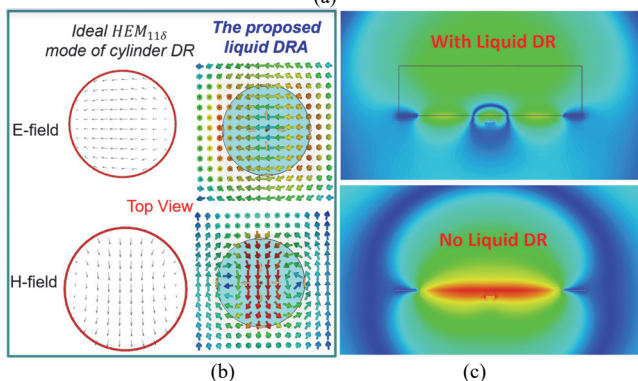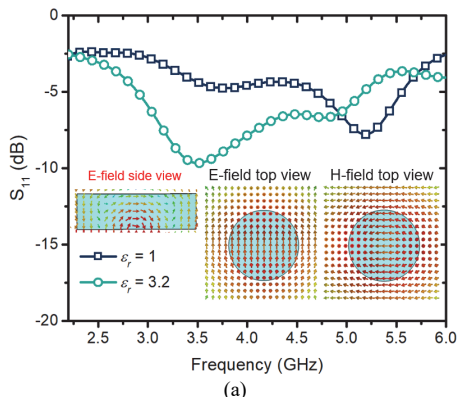

(a)

(b)   (c)

Fig. 4. (a) Comparison between the simulated S_{11} of the proposed DRA and a free-space slot antenna. The simulated E-field and H-field distributions at 3.5 GHz of the DRA are given. (b) Top view of E-field and H-field of the proposed liquid DRA at 3.5 GHz and the ideal $HEM_{11\delta}$ mode of cylinder DR [23]. (c) Comparison of the E-field side views of the proposed antenna with and without using the liquid DR at 3.5 GHz.
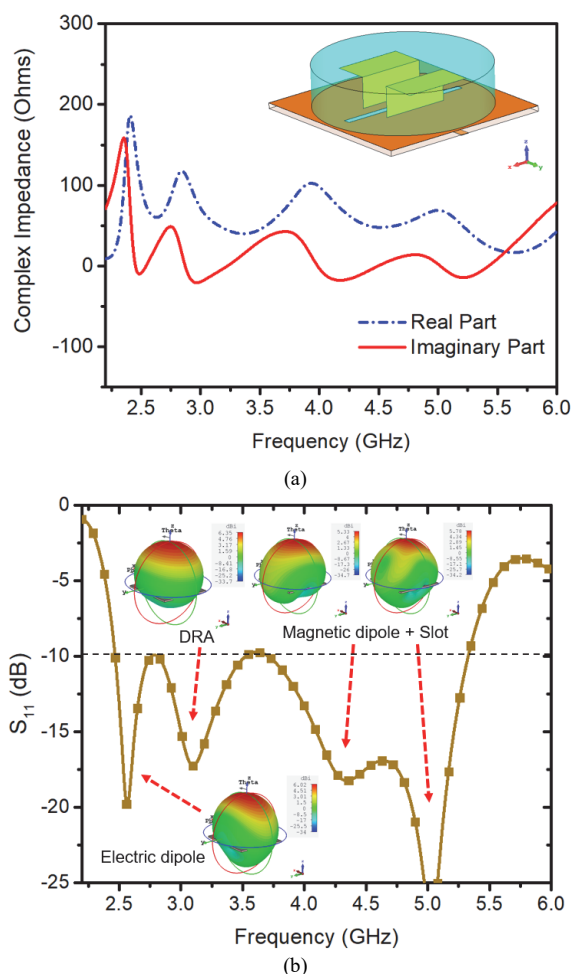

(a)

(b)

Fig. 5. Simulated (a) input impedance and (b) S_{11} of the proposed hybrid antenna. The 3D radiation patterns at 2.6 GHz, 3.1 GHz, 4.2 GHz and 5 GHz are shown as well.

proposed antenna are presented. Finally, an experimental prototype of the proposed antenna has achieved a frequency coverage of 2.45 – 5.3 GHz, a realized gain > 5 dBi, a stable broadside radiation pattern, a wide beam-width and low back radiation levels over the desired frequency band. It has combined the advantages of both DRA and ME-dipole (e.g., bandwidth > 70% and a very small overall dimension of 0.42 ×0.42×0.11 $\lambda_0{}^3$ at 2.45 GHz), which shows significant advantages over existing ME dipole antennas and DRAs in terms of size, bandwidth, and overall simplicity. The antenna design could also be expanded for other antenna structures.

The rest of this paper is organized as follows. The antenna geometry is introduced in Section II. The analysis of the multiple resonant modes and design guideline of the hybrid antenna are presented in Section III. The antenna performance validations and discussions are given in Sections IV. Finally, conclusions are drawn in Section V.

II. ANTENNA STRUCTURE AND DIMENSIONS

Fig. 1 (a) depicts the disassembled view of the proposed antenna that consists of an ME dipole, a liquid DRA, an aperture-fed PCB and a 3D printed resin container. The PCB is

built on an FR4 substrate with a relative permittivity of 4.4 and a thickness of 1.57 mm. The geometry and notations of the antenna parameters are given in Fig. 1 (b). The ME dipole and DRA are excited simultaneously by using the aperture-fed scheme where the feeding slot can be characterized as a magnetic dipole equivalence. The resin container has a wall thickness of 0.8 mm and a relative permittivity of around 3. The optimized parameters of an example of the proposed hybrid antenna are listed in Table I. The overall dimension of the antenna is $52 \times 52 \times 13.6$ mm^3.

III. HYBRID MULTIPLE RESONANT MODES ANALYSIS

A. ME Dipole Mode

To analyse the resonant modes of the hybrid antenna, we firstly study a single ME dipole without loading the liquid. It is worth noting that the operating principle of this antenna is slightly different from that of the traditional probe-fed ME dipole, where the vertically shorted patch is the main factor for producing the magnetic dipole resonance. In our design, the ME-dipole is aperture-fed, and the feeding slot can be seen as a magnetic dipole equivalence, which becomes the dominant factor for the magnetic dipole resonance. The comparison between the probe-fed and aperture-fed electric dipole is shown in Fig. 2 (a) in terms of the signal excitation location. It can be seen that the electric dipole is excited at the top of the vertical patch (in parallel to horizontal dipole arm) when a probe feed is used. In this case the electric dipole length will be about the length of the horizontal arm ($2 \times L1$). In contrast, since the aperture feed of our design is located at the bottom of the vertical patch on the ground plane, therefore the excitation location of the electric dipole will be lower than that of the probe-fed case, in which the height of the vertical patch will be taken into consideration to determine the electric dipole length [$2\times(L1+H2)$]. The simulated input impedance and reflection coefficient S_{11} of the aperture-fed ME dipole are depicted in Figs. 2 (b) and (c). The dimensions of the antenna are identical to the design parameters given in Table I. From Fig. 2 (b), it can be seen that two effective resonances are realized at 4.3 GHz and 5 GHz, respectively. The resonance at around 3.2 GHz exhibits an anti-resonant behaviour (poor impedance matching) since the imaginary part of the impedance decreases dramatically from 170 to -120 Ω.

According to the operation mechanism of the ME-dipole [22], the former resonance (at 4.3 GHz) is due to the electric dipole resonance while the latter (at 5 GHz) is originated from the magnetic dipole. As a validation, we measured the electric dipole length of the proposed aperture-fed ME-dipole, which is $2 \times (L1 + H2) = 38$ mm (about 1/2 λ_0 at 4.3 GHz). The length of the feeding slot (magnetic dipole length L3 = 40 mm) is around 0.66 λ_0 at 5 GHz. From our parametric study results (not shown here), we found that the 4.3 GHz resonance is very sensitive to the variation of L1 and H2, which shows that it is the electric dipole resonance. While the resonance at 5 GHz was found to be independent of L1 and H2, but it is determined mainly by the size of the feeding slot L3. Consequently, it is evident that 5 GHz resonance is a magnetic dipole resonance. Moreover, we found that the antenna bandwidth is a function of H2 and L1, the larger the two parameters, the wider the

bandwidth. Herein, since the size of the dipole arm is relatively small, thus the realized bandwidth is narrow than that of the traditional ME-dipoles with higher profiles and larger dimensions. The impedance bandwidth for $S_{11} <$ -10 dB is about 4.1 – 5.3 GHz with a corresponding fractional bandwidth (FBW) of 25.5% (see Fig. 2 (b)). The overall electrical size of the antenna at the centre frequency of 4.7 GHz is around $0.81 \times 0.81 \times 0.17$ λ_0^3. The antenna bandwidth of such an aperture-fed ME dipole can be significantly broadened by enlarging the sizes of e.g., electric dipole length (L1), magnetic dipole length (L3) and antenna height (H2) [22]. However, here we would like to study a relatively basic example using standard ME-dipole structures with a smaller dimension and subsequently show the frequency band improvement without increasing the antenna size and/or modifying the antenna structure significantly by using the hybrid antenna technology (to be introduced in the following sections). The simulated 3D radiation patterns at 4.3 and 5 GHz are given in Fig. 2 (c). It can be seen that the desired unidirectional broadside radiation pattern of the ME-dipole antenna is achieved. The E-plane and H-plane radiation patterns are not perfectly symmetrical due to the aperture feed and the smaller ground plane, but the shape of the pattern still follows that of the ME-dipole antennas.

B. DRA Mode

The ME dipole is aperture-coupled, in which the feeding slot can also be used to excite the $HEM_{11\delta}$ mode of a cylindrical DRA. Herein, we investigate the case of DRA only, where the ME dipole antenna is removed. A dielectric material with a relatively low permittivity will be selected to reduce the quality factor (Q-factor) and maintain the overall impedance bandwidth of the hybrid antenna. The design parameters in Table I are also used to build the cylinder DRA. A low-loss ionic liquid, trihexyltetradecylphosphonium chloride, with a relative permittivity of 3.2 is selected [18]; also see Section IV. Such low permittivity materials (e.g., PVC) have already been used to develop low-Q wideband DRA via the combination of the DRA mode and dielectric loading effect [24]. To predict the theoretical resonant frequency and Q-factor of the cylindrical DRA, the following equations can be used [23].

$$k_0 r = \frac{6.324}{\sqrt{\varepsilon_r + 2}} \{0.27 + 0.36(x/2) - 0.02(x/2)^2\} \quad (1)$$

$$Q = 0.01007 \varepsilon_r^{1.3} x \{1 + 100 e^{-2.05(x/2 - x^2/80)}\} \quad (2)$$

$$k_0 r = \frac{f_{GHz} \cdot h_{cm} \cdot x}{4.7713} \quad (3)$$

where $x = r / h$, r is the radius of the DRA ($0.5 \times R1 = 25$ mm), h is the height of the DRA (H1= 12 mm), h_{cm} is the value (without units) of h in centimeters and $\varepsilon_r = 3.2$. By using (1) and (3), the calculated resonant frequency at the $HEM_{11\delta}$ mode is 3.8 GHz. Using (2), an estimated Q-factor of 1.37 can be obtained. Therefore, the frequency bandwidth of the DRA is approximately 3.8 GHz/Q = 2.77 GHz, where the band starts from 2.42 GHz and stops at 5.19 GHz. The simulated input impedance and S_{11} of the liquid DRA is shown in Figs. 3 (a) and (b). It can be seen that the main resonant frequency is located at around 3.5 GHz with a frequency band coverage of 3 – 5 GHz. The extra resonance at 5 GHz is likely due to the slot mode of the feeding aperture [23]. The impedance matching over the bandwidth is not very good, resulting in an average S_{11} level
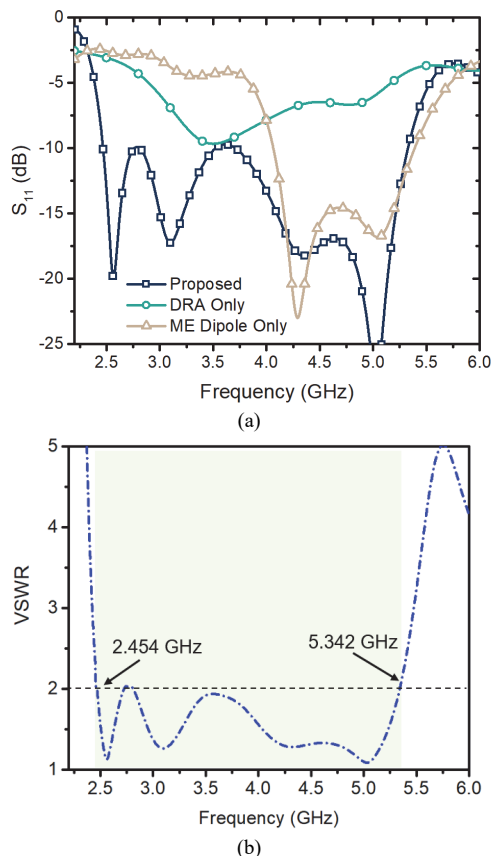
Fig. 6. (a) Comparison between the three different antennas. (b) Simulated VSWR of the proposed hybrid antenna.

between –6 dB and –10 dB. This might be due to the utilization of the low permittivity material. To verify the existence of the DRA mode at around 3.5 GHz, we firstly study the DRA with different relative permittivity values, as shown in Fig. 4 (a). When $\varepsilon_r = 1$ (free space), the resonance at around 5 GHz (slot mode) still remains but the mode at 3.5 GHz is not obvious (poorly matched). In addition, the top views of the simulated E-field and H-field and side view of the E-field at 3.5 GHz of the propose DRA are depicted in Fig. 4 (a). Furthermore, we have compared the field distribution of the liquid DR with that of the ideal $HEM_{11\delta}$ mode of the cylindrical DRA (see Fig. 4 (b)). The field distributions are identical to that of the $HEM_{11\delta}$ mode cylindrical DRA which verifies the existence of the DRA mode at 3.5 GHz. If the liquid DR is removed, the electric field will propagate on both sides of the slot at 3.5 GHz, which means that the antenna is under the slot mode. However, after adding the liquid DR, the E-field at 3.5 GHz only propagates to a single direction with very small backward radiation (see Fig. 4 (c)). This demonstrates that the desired E-field of $HEM_{11\delta}$ mode cylindrical DRA has been excited to replace the slot mode at 3.5 GHz, making the proposed antenna a unidirectional radiator. The overall electrical size of the antenna at the centre frequency of 4 GHz is around $0.69 \times 0.69 \times 0.17 \, \lambda_0{}^3$.

The simulated 3D radiation patterns of the DRA at 3.5 and 5 GHz are also provided in Fig. 3. The desired unidirectional broadside radiation patterns for the $HEM_{11\delta}$ mode are realized at both frequencies. The backward radiation at 5 GHz is larger than that at 3.5 GHz as expected from a slot radiator [30].
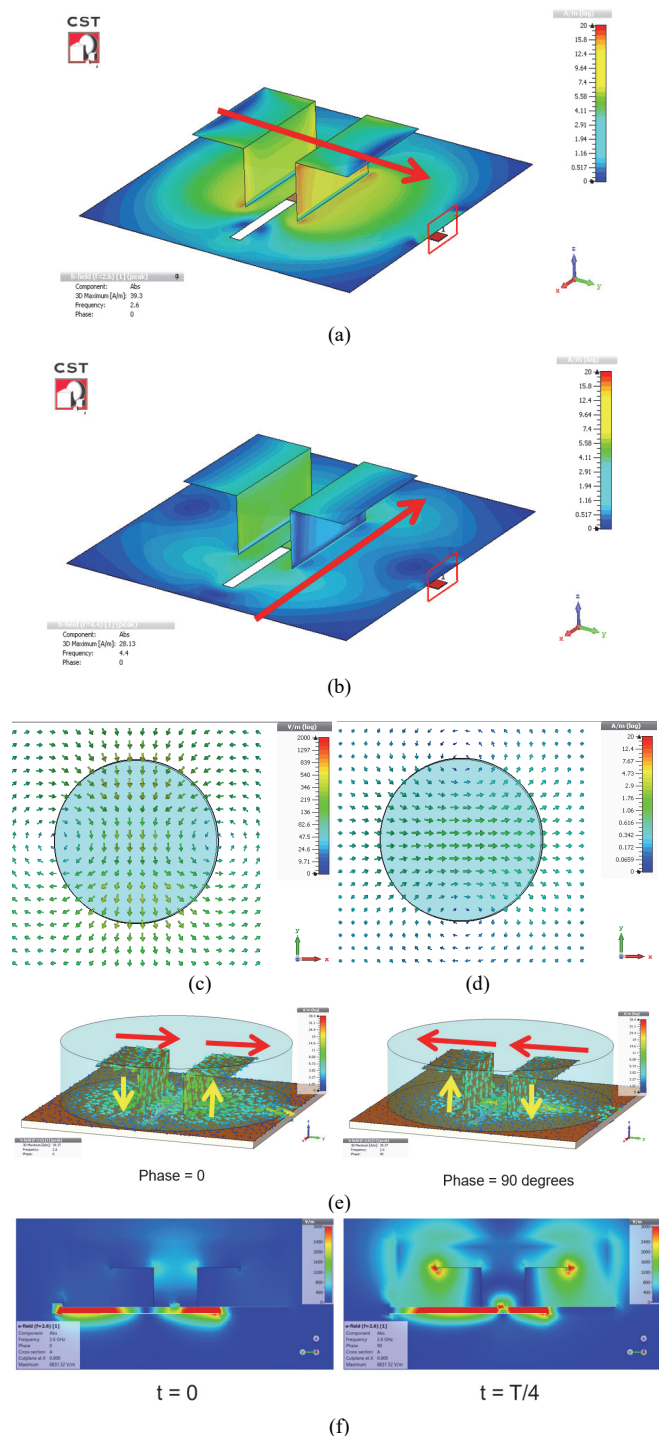

Fig. 7. (a) Simulated surface current distribution at 2.6 GHz. (b) Simulated surface current distribution at 4.4 GHz. (c) Top view of the E-field distribution at 3.1 GHz. (d) Top view of the H-field distribution at 3.1 GHz. (e) Simulated vector current distribution at two different phase angles. The current directions have been marked. (f) Electric-field side views at different periods of time.

C. Mode Combination of the Hybrid Antenna

If the aforementioned ME dipole and DRA are strategically combined, multi-resonant modes could be realized so that the DRA and ME dipole can co-operate over a wider frequency band with a smaller overall dimension. The hybrid antenna will combine the advantages of both DRA and ME dipole and

meanwhile overcoming their drawbacks. The simulated input impedance of the proposed hybrid antenna is given in Fig. 5 (a). It can be clearly seen that there are four resonances realized at around 2.5 GHz, 3 GHz, 4.2 GHz and 5 GHz respectively. The number of resonances of the proposed hybrid antenna is greater than that of the single ME-dipole and single DRA (as depicted in Figs. 2 (a) and 3 (a)). This shows that the resonances of the hybrid antenna over the frequency band of interest is the combination of the ME-dipole and DRA resonances. The simulated reflection coefficient S_{11} of the proposed hybrid antenna is depicted in Fig. 5 (b). It can be seen that the proposed antenna has a much wider impedance bandwidth than the single DRA and ME dipole. The antenna covers from 2.45 to 5.3 GHz with an FBW of 73.5%. In addition, four major resonances are realized within the band, locating at 2.6 GHz, 3.1 GHz, 4.2 GHz and 5 GHz respectively. The 3D radiation patterns at these four frequencies are shown in Fig. 5 (b) as well. It can be seen that the patterns at 2.6, 4.2 and 5 GHz are likely to be the radiation patterns of the ME dipole. While the pattern at 3.1 GHz is similar to that of the $HEM_{11\delta}$ mode DRA. But in general, the antenna has achieved the broadside unidirectional radiation with a relatively wide beam-width and high gain over such a wide band.

The comparison between the single ME dipole, single DRA and the proposed antenna is shown in Fig. 6 (a). The proposed antenna has combined four resonant modes originated from the electric dipole, magnetic dipole, DRA, and feeding slot (magnetic dipole equivalence) respectively. The simulated VSWR of the final antenna is depicted in Fig. 6 (b). The value of VWSR is generally less than 2 across the frequency band of interest. To understand the underlying mechanism of each mode, we show the current distributions at 2.6 and 4.4 GHz in Figs. 7 (a) and (b). It can be seen that the resonance at around 2.6 GHz is due to the electric dipole mode since the current propagates along the direction of the horizontal electric dipole arms (marked using an arrow). In contrast, the resonance at around 4.4 GHz is generated by the magnetic dipole as the current travels along the direction of the feeding slot and the magnetic dipole arm (marked using an arrow).

Moreover, the top views of the E-field and H-field distributions at 3.1 GHz are given in Figs. 7 (c) and (d). Such field distributions are identical to that of the ideal cylindrical DRA at the $HEM_{11\delta}$ mode which future verifies the existence of the DRA mode of the hybrid antenna. The vector current distribution of the antenna at two different phase angles is given in Fig. 7 (e) and the side views of the electric field distributions at different periods of time are depicted in Fig. 7 (f). The current directions on the horizontal dipole arms and vertical shorted patches have been respectively marked using different arrows. At phase = 0° (or t = 0), the horizontal current on the planar dipole is dominated in one direction where the currents with quasi-sinusoidal distribution on the planar electric dipoles are found to be maximum. Meanwhile, the electric field at the aperture slot reaches its maximum value as the vertical currents on shorted quarter-wave patches are minimized. In contrast, at phase = 90° (or t = T /4, where T is a period of time) the horizontal currents and the aperture electric field are minimized, while vertical currents on the shorted patch are strongly excited.
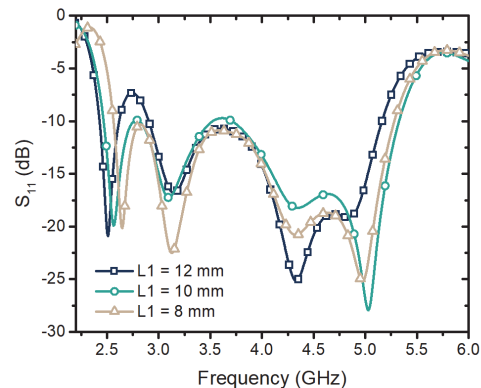

Fig. 8. Simulated S_{11} of the proposed hybrid antenna by changing the value of L1.
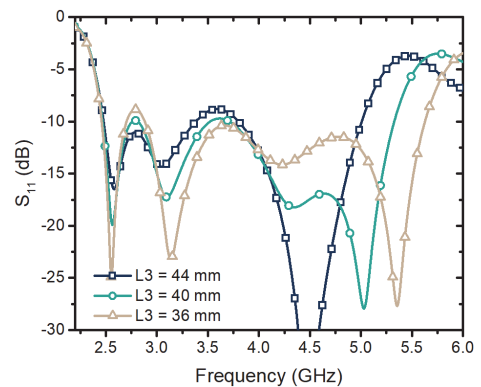

Fig. 9. Simulated S_{11} of the proposed hybrid antenna by changing the value of L3.
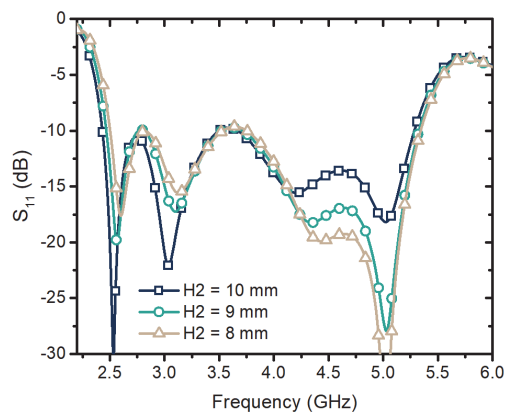

Fig. 10. Simulated S_{11} of the proposed hybrid antenna by changing the value of H2.
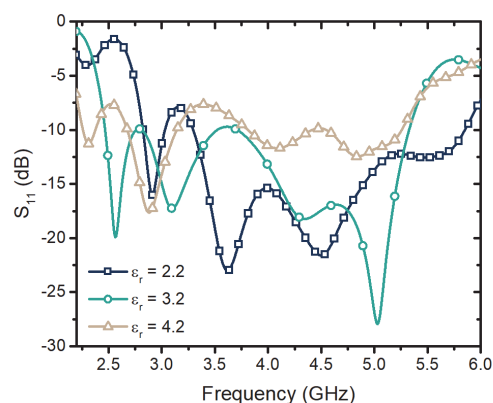

Fig. 11. Simulated S_{11} of the proposed hybrid antenna by changing the relative permittivity of the liquid DRA.

The above analysis indicates that the electric dipole and magnetic dipole are excited simultaneously with in-phase radiations [31]; therefore, demonstrating the ME dipole concept of the proposed antenna. Parametric studies have also been conducted to understand the impact on antenna performance by changing the vital design parameters. Fig. 8 shows the results of S_{11} by using different values of L1. It can be seen that the variation of L1 has caused a major effect on the electric dipole resonance at around 2.5 GHz. This verifies the antenna mechanism since the length of the electric dipole arm is mainly determined by L1. Similarly, when the length of the feeding slot L3 is varying, significant impact can be observed at the magnetic dipole resonant band at around 5 GHz (see Fig. 9). While the height of the shorted patch (H2) will have a major impact to the resonance at around 4.5 GHz (see Fig. 10). Lastly, if the relative permittivity of the DRA is varying, the resonance at around 3 GHz changes quite significantly (see Fig. 11). It is worth noting that the permittivity of the DR would also influence the overall performance of the proposed antenna. In summary, the proposed antenna has realized a much wider bandwidth (73.5%) with a relatively small size of $52 \times 52 \times 13.6$ mm^3 ($0.66 \times 0.66 \times 0.16 \lambda_0^3$ at the centre frequency of 3.85 GHz) through the combination of DRA and ME dipole.

Importantly, the DR may act as a dielectric loading that has shifted the electric dipole resonance from 4.3 to 2.5 GHz (by an order of around $\sqrt{\varepsilon_r}$). But the dielectric loading does not significantly affect the magnetic dipole resonance (at 4.5– 5 GHz). This is different from the conventional dielectric loaded antennas. One major reason is that the M-dipole is not fully loaded by the dielectric liquid. The aperture slot is located at the bottom of the liquid block, therefore, only half of the electric field generated from the M-dipole (slot) will be affected by the dielectric medium before propagating into the free space (see Fig. 4 (c)). In contrast, the E-dipole arm is fully immersed into the liquid thus it has been fully loaded. All electric fields generated from the E-dipole will propagation through the dielectric medium before going into the air. Consequently, in our antenna model, only E-dipole resonance is shifted due to the dielectric loading, while the M-dipole resonance has been maintained. Therefore, the antenna could realize a very wide bandwidth via the means of multi-resonant mode combination. We have summarized these new findings as the mode combination principle of the proposed antenna in Fig. 12. The design guideline is given as follows.

1) First of all, design an ME dipole with two major resonances by choosing appropriate sizes for the horizontal dipole arms and vertically shorted patches in accordance with the operating frequency.

2) Secondly, develop a low-permittivity DRA with a broadside radiation pattern and a resonant frequency slightly lower than the lowest frequency of the previously designed ME-dipole.

3) Loading the ME-dipole with the DRA and tune the parameters of the electric dipole (L1, D1), magnetic dipole (H2, W1), and feeding slot (L3, W3) for the right frequency coverage.

Another important investigation in this work is to study the effect on antenna performance when using a larger ground plane, as the antenna might be installed over large metallic
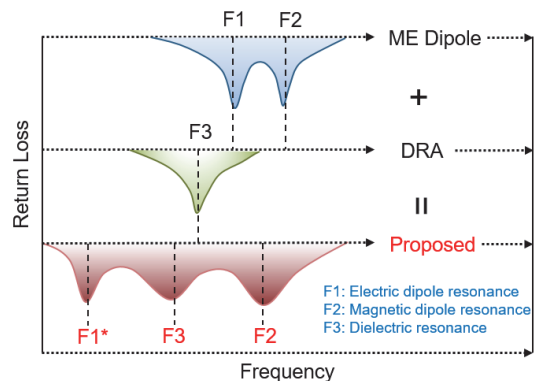

Fig. 12. Combination of the hybrid multiple resonant modes. For simplicity, the feeding slot mode is combined as magnetic dipole resonance.
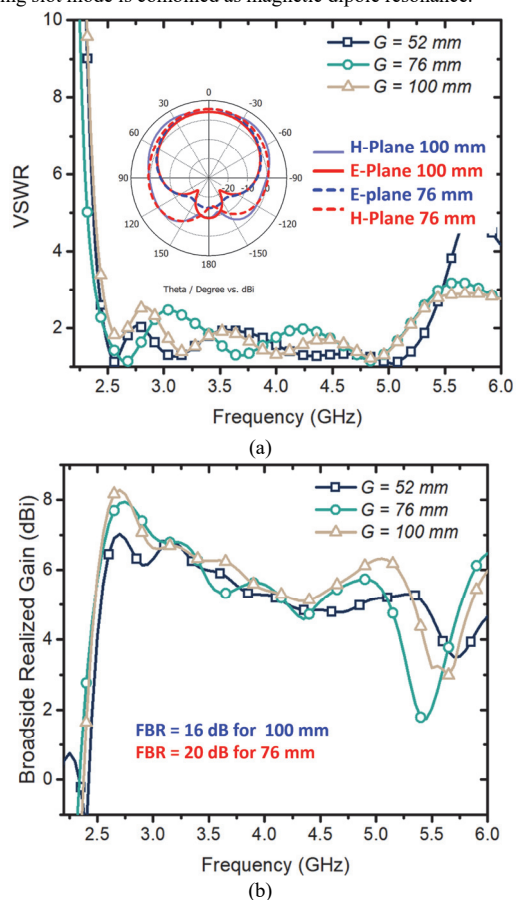

(a)

(b)

Fig. 13. (a) VSWR and (b) broadside realized gain of the proposed hybrid antenna with different ground plane sizes. The 2D radiation patterns of the antenna at the centre frequency of 3.8 GHz are shown for 76 mm and 100 mm ground plane respectively.

surfaces (e.g., vehicle top) in practice. As can be seen from Fig. 13, the VSWR and broadside realized gain of the antenna are reasonably stable when the ground plane size is increased from G = 52 mm to G = 100 mm. Slight difference can be observed on the VSWR at 3 – 3.5 GHz. In addition, the E-plane and H-plane radiation patterns at the centre frequency of 3.8 GHz are depicted in Fig. 13 for 76×76 mm^2 and 100×100 mm^2 ground plane respectively. It is found that the symmetry of radiation pattern is improved slightly. The front-to-back ratios (FBR) are about 20 dB and 16 dB for the ground plane length equal to 76 mm and 100 mm respectively.

It should be emphasised that, the design example in this paper has used the most typical ME-dipole structure. The aim is to show the feasibility of the proposed hybrid antenna scheme. Other ME-dipoles with modified structures for horizontal arms, vertical patches and feeding structures [25]-[29] could also be considered for the hybrid antenna design by using the liquid dielectric in this work. In these scenarios, more compact dimensions and wider impedance bandwidth could be realized.

IV. EXPERIMENTAL VALIDATIONS AND PERFORMANCE COMPARISON

A. Antenna Fabrication

We have fabricated a prototype of the proposed antenna using the optimized dimensions provided in Table I. A picture of the antenna prototype is shown in Fig. 14. The resin container was filled with the liquid material and sealed to the PCB by using silicone gels. The liquid material used in this work, trihexyltetradecylphosphonium chloride, is a special ionic liquid which has been presented in our previous work [18]. It remains liquid over a very large temperature range [−69.8 °C (glass transition) to +350 °C (decomposition)], and it has a relative permittivity of around 3.1, an extremely low dielectric loss (loss tangent < 0.04), and very stable thermophysical material properties. This ionic liquid has been tested at our lab under -65°C which showed that the liquid state remained stable without significant volume changes. In addition, the liquid is not flammable and does not vaporize. The experimental results have shown that this liquid has a stable performance (in terms of permittivity and loss tangent) over a wide temperature range from −20 to 60 °C (using typical lab heating blocks and cryogenic cooling) as well as a wide frequency range from 2 GHz to 6 GHz (see Fig. 15).

B. Experimental Validations

The measured S_{11} of the proposed antenna is given in Fig. 16 along with the simulated ones. In general, good agreements have been obtained while the measured antenna performance is quite stable over a wide range of temperature. Furthermore, the simulated and measured total efficiency and realized gains of the antenna are depicted in Fig. 17. It can be seen that the proposed antenna has a relatively stable gain of $4.8 - 7$ dBi over the wide frequency band from 2.5 to 5.3 GHz. The antenna efficiency is above 80% for the frequency band of interest. In addition, the measured and simulated 2D radiation patterns over E-plane and H-plane are shown in Fig. 18 at four major resonant frequencies. The co-polarization and cross-polarization 3D patterns are given as references. It is shown that the antenna has achieved a broadside radiation pattern over the entire frequency band with complementary radiation patterns. The E-plane and H-plane patterns are quite symmetrical with a wide beam-width of around 120°, 100°, 90° and 80° at frequency bands of 2.5, 3.1, 4.2 and 5 GHz respectively. Therefore, the proposed hybrid antenna has taken the advantageous features of both ME dipole and DRA. The measured front-to-back ratios of the proposed antenna are around 25 dB (at 2.6 GHz), 20 dB (at 3.1 GHz), 18 dB (at 4.2 GHz) and 9 dB (at 5 GHz) respectively. The back radiation at 5 GHz is increased which is due to the slot mode effect at higher frequencies. The backward radiation of such
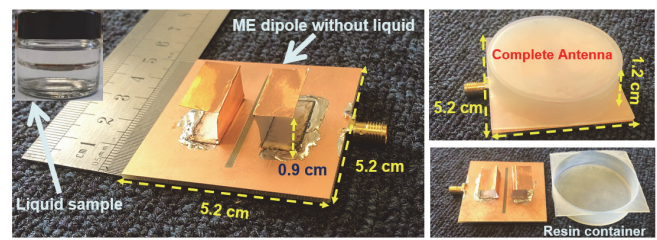

Fig. 14. Fabricated prototype of the proposed hybrid liquid DR and ME-dipole antenna.

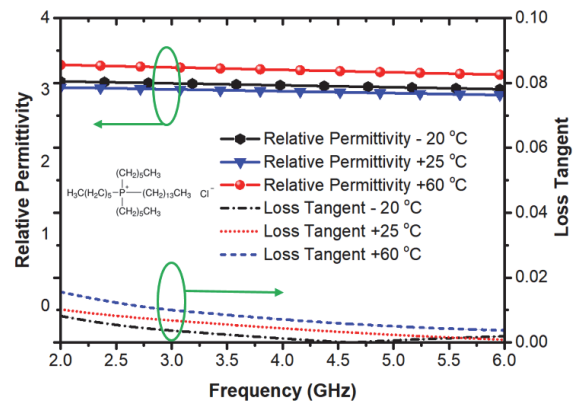Fig. 15. Measured relative permittivity and loss tangent of the proposed ionic liquid over a temperature range from -20 to +60 °C.
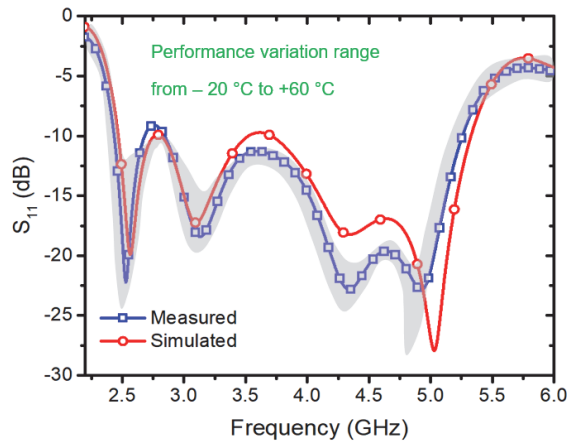

Fig. 16. Measured and simulated S_{11} of the proposed hybrid antenna. The performance variation vs. a wide temperature range (from -20 to +60 °C) is presented.
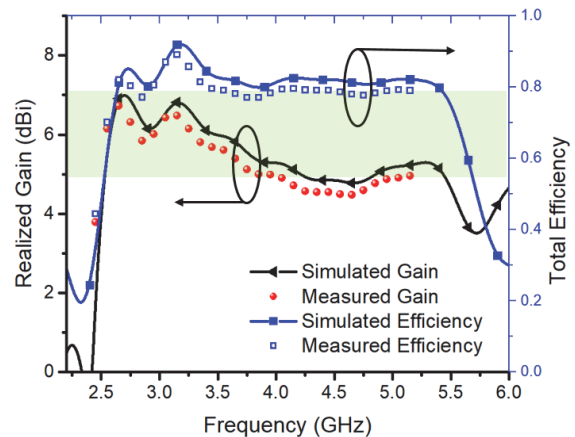

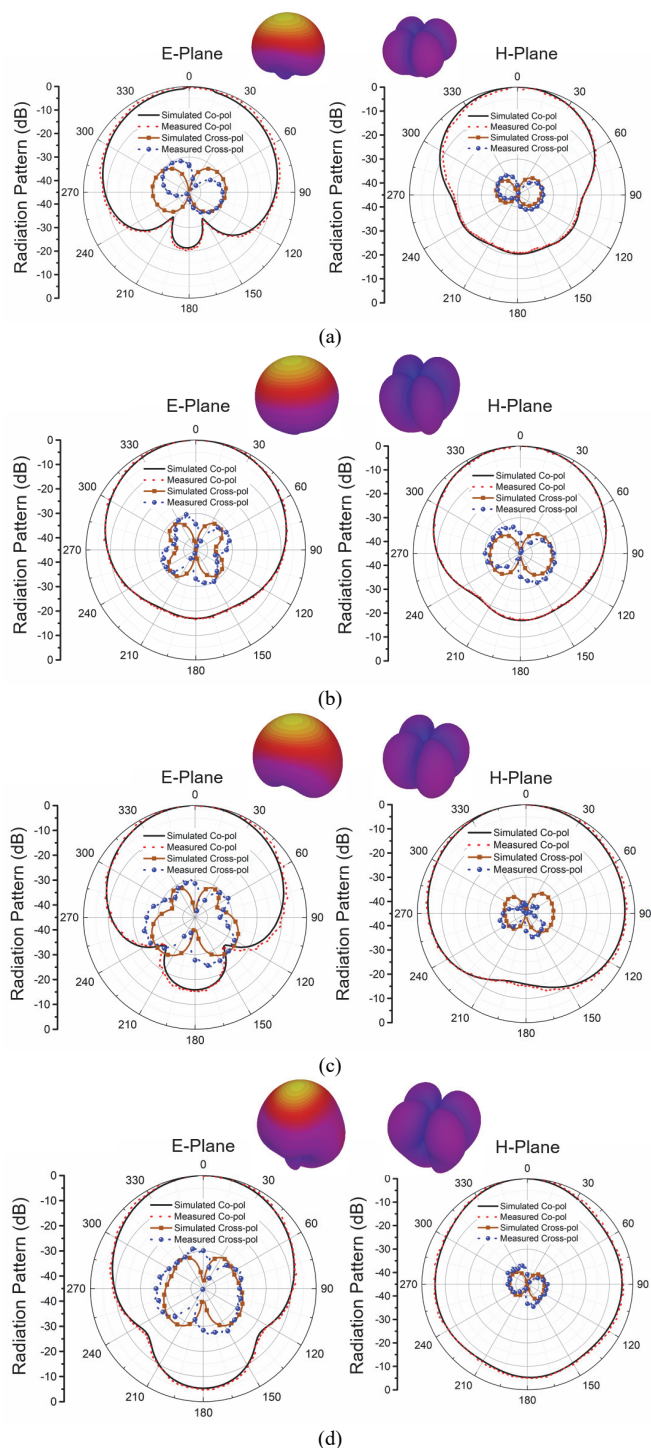Fig. 17. Measured and simulated broadside realized gain and total efficiency of the proposed hybrid antenna.

Fig. 18. Measured and simulated 2D radiation patterns over E-plane and H-pane at (a) 2.6 GHz, (b) 3.1 GHz, (c) 4.2 GHz and (d) 5 GHz. The co-polarization and cross-polarization 3D patterns are given as references.

aperture-fed ME dipole antennas can be reduced by either using a larger ground plane (as shown in Fig. 13) or adding additional reflective layers (e.g., AMC and EBG) underneath the antenna [30].

C. Performance Comparison

The performance comparison between the proposed hybrid antenna and other related ME-dipole antenna designs is given in Table II. It can be seen that our antenna has achieved a reasonably compact dimension. The electrical size of the ME-dipole radiator of our antenna is just $0.39\lambda_0\times0.26\lambda_0\times0.117\lambda_0$ while the size of the liquid DR radiator is about $0.64\lambda_0\times0.64\lambda_0\times0.155\lambda_0$ where λ_0 represents the wavelength at 3.875 GHz (centre frequency). In addition, the proposed design has achieved a very wide impedance bandwidth with a reasonable radiation pattern, gain, and structural complexity. The realized bandwidth of this work is much wider than that of the dielectric-based [12], dielectric-loaded [11] and metamaterial-loaded [10] ME dipole designs. This has shown the advancements of the proposed multi-resonant modes combination scheme over the conventional design approaches. The initial bandwidth of the standard ME-dipole was 25.5% which has been broadened to 73.5% after using the hybrid DR and ME dipole design. Compared with those UWB ME-dipole designs with over 100% bandwidth [26]-[28], our design has realized a relatively small radiator dimension (without considering the ground plane size) and simpler structures. By mixing the ME dipole with a liquid DRA, the loading effect has significantly reduced the demand for a large ground plane to maintain the pattern and gain performance of the antenna. If the antenna size is evaluated at the lowest resonant frequency (2.45 GHz), the proposed antenna has an overall dimension of $0.42 \times 0.42 \times 0.11 \lambda_0^3$, which is compact and of low-profile for such wideband antennas with a stable broadside radiation. Importantly, the design in this paper is just an example to show the advantage of this novel hybrid antenna scheme. It should be emphasised that the ME-dipole radiator of this work is based on a very standard design which has a limited bandwidth and performance. After using the hybrid technology, it has shown significant performance improvement without modifying the antenna structure significantly. The gain range of the hybrid antenna is slightly lower than that of the original ME-dipole example without using the DRA. This is because that the hybrid antenna has realized a lower resonant frequency band (after the DR loading); therefore, the original ground plane of the ME-dipole will need to be enlarged for higher gains. Also, the gain of the proposed antenna is affected by the backward radiation at higher frequencies. The proposed design can be further modified to dual-linear polarization and/or circular polarization by using different feeding apertures, while its bandwidth and antenna size can be further improved by using modified ME-dipole structures in such as [25]-[29].

V. CONCLUSION

A novel hybrid antenna that consists of a liquid DRA and an ME dipole has been presented. Different from the traditional DRAs, ME dipoles and dielectric-loaded antennas, the proposed antenna has strategically combined four different resonant modes originated from the electric dipole, magnetic dipole, DRA and the feeding aperture, respectively. As a consequence, the realized bandwidth of the hybrid antenna has been significantly broadened while the overall antenna dimension has been much reduced. We have theoretically proven and experimentally demonstrated a prototype of the proposed antenna that has realized a bandwidth of 73.5%, a realized gain between 5 and 7 dBi, a front-to-back ratio lower

TABLE II
COMPARISON OF THE PROPOSED HYBRID ANTENNA AND RELATED DESIGNS

Ref. (year)	Impedance bandwidth (GHz)	Fractional bandwidth	Realized gain range over the band (dBi)	Overall complexity	SR: size of the ME-dipole radiator SD: size of the dielectric resonator SC: size of complete antenna	
					Electrical size (λ_0 refers to the free-space wavelength at center frequency)	Physical size (unit: mm^3)
[4] (2018)	3.3 – 7.8	81.1%	3.7 ~ 5.3	medium	SR: $0.37\lambda_0\times0.44\lambda_0\times0.296\lambda_0$ SC: $0.74\lambda_0\times0.74\lambda_0\times0.296\lambda_0$	SR: 20 × 24 × 16 SC: 40 × 40 × 16
[8] (2013)	1.86 – 2.96	45.6%	7 ~ 8.1	complex	SR: $0.48\lambda_0\times0.51\lambda_0\times0.169\lambda_0$ SC: $1.04\lambda_0\times1.04\lambda_0\times0.169\lambda_0$	SR: 60 × 64 × 21 SC: 130 × 130 × 21
[9] (2016)	1.67 – 2.22	28.2%	8 ~ 10	complex	SR: $0.51\lambda_0\times0.93\lambda_0\times0.097\lambda_0$ SC: $1.00\ \lambda_0\times1.00\ \lambda_0\times0.097\lambda_0$	SR: 79 × 143 × 15 SC: 152 × 152 × 15
[10] (2016)	1.7 – 2.67	44%	7.8 ~ 8.5	complex	SR: $0.36\lambda_0\times0.52\lambda_0\times0.197\lambda_0$ SC: $1.09\lambda_0\times1.09\lambda_0\times0.197\lambda_0$	SR: 50 × 71 × 27 SC: 150 × 150 × 27
[22] (2018)	2.6 – 6.2	85%	5 ~ 8	simple	SR: $0.62\lambda_0\times0.68\lambda_0\times0.23\lambda_0$ SC: $1.64\lambda_0\times1.64\lambda_0\times0.23\lambda_0$	SR: 45 × 50 × 17 SC: 120 × 120 × 17
[25] 2018	1.38 – 3.5	86.9%	6 ~ 8.4	simple	SR: $0.53\lambda_0\times0.59\lambda_0\times0.227\lambda_0$ SC: $1.46\lambda_0\times1.46\lambda_0\times0.227\lambda_0$	SC: 65 × 73 × 28 SC: 180 × 180 × 28
[26] 2017	3.1 – 10.66	110%	5.9 ~ 10.9	complex	SR: $1.44\ \lambda_0\times0.57\lambda_0\times0.27\lambda_0$ SC: $2.10\lambda_0\times1.10\lambda_0\times0.27\lambda_0$	SR: 42.5 × 16.85 × 8 SC: 62 × 32.5 × 8
[27] 2013	2.95 – 10.73	114%	8.2 ~ 9.3	complex	SR: $0.59\ \lambda_0\times0.86\lambda_0\times0.359\lambda_0$ SC: $1.48\lambda_0\times1.48\lambda_0\times0.359\lambda_0$	SR: 26 × 38 × 15.8 SC: 65 × 65 × 15.8
[28] 2013	3.08 – 10.6	110%	6.8 ~ 10.6	complex	SR: $0.92\ \lambda_0\times0.58\lambda_0\times0.274\lambda_0$ SC: $1.48\lambda_0\times1.11\lambda_0\times0.283\lambda_0$	SR: 40.4 × 25.4 × 12 SC: 65 × 50 × 12.4
[29] 2012	1.88 – 3.3	54.8%	7.8 ~ 9.4	medium	SR: $0.52\ \lambda_0\times0.57\lambda_0\times0.164\lambda_0$ SC: $0.97\lambda_0\times0.97\lambda_0\times0.173\lambda_0$	SR: 60 × 65.4 × 19 SC: 112 × 112 × 20
This work (2019)	**4.1 – 5.3*** **2.45 – 5.3****	**25.5%*** **73.5%****	**7.5 ~ 8.2*** **5 ~ 7****	**simple**	**SR: $0.39\lambda_0\times0.26\lambda_0\times0.117\lambda_0$** **SD: $0.64\lambda_0\times0.64\lambda_0\times0.155\lambda_0$** **SC: $0.66\lambda_0\times0.66\lambda_0\times0.167\lambda_0$**	SR: 30 × 20 × 9 SD: 50 × 50 × 12 SC: 52 × 52 × 13.6

*ME-dipole only
** Hybrid antenna

than 15 dB, broadside radiation patterns and a relatively wide beam width over the operating frequency band from 2.45 to 5.3 GHz. Most importantly, the antenna was based on a standard aperture-fed ME-dipole with a quite compact size and less-complicated structures. The electrical size of the final antenna is only $0.42 \times 0.42 \times 0.11\ \lambda_0^3$ at 2.45 GHz. This hybrid antenna has combined the advantages from both DRAs and ME dipoles and meanwhile overcoming their drawbacks. The proposed hybrid antenna scheme can be further developed for compact mobile base station applications and 5G communication systems. This work has shown the great potential for a new class of compact wideband antennas by combing the liquid dielectrics and traditional metal antennas (e.g. dipole, patch, and loop etc.).

REFERENCES

[1] T. S. Rappaport, Y. Xing, G. R. MacCartney, A. F. Molisch, E. Mellios and J. Zhang, "Overview of Millimeter Wave Communications for Fifth-Generation (5G) Wireless Networks—With a Focus on Propagation Models," *IEEE Transactions on Antennas and Propagation*, vol. 65, no. 12, pp. 6213-6230, Dec. 2017.

[2] K. M. Luk and H. Wong, "A new wideband unidirectional antenna element," *Int. J. Microw. Opt. Technol.*, vol. 1, no. 1, pp. 35–44, Jun. 2006.

[3] J. Zeng and K. Luk, "Single-Layered Broadband Magnetoelectric Dipole Antenna for New 5G Application," *IEEE Antennas and Wireless Propagation Letters*, vol. 18, no. 5, pp. 911-915, May 2019.

[4] G. Yang, J. Li, J. Yang and S. Zhou, "A Wide Beamwidth and Wideband Magnetoelectric Dipole Antenna," *IEEE Transactions on Antennas and Propagation*, vol. 66, no. 12, pp. 6724-6733, Dec. 2018.

[5] A. Kaddour, S. Bories, A. Bellion and C. Delaveaud, "3-D-Printed Compact Wideband Magnetoelectric Dipoles with Circular Polarization," *IEEE Antennas and Wireless Propagation Letters*, vol. 17, no. 11, pp. 2026-2030, Nov. 2018.

[6] D. Shen, C. Ma, W. Ren, X. Zhang, Z. Ma and R. Qian, "A Low-Profile Substrate-Integrated-Gap-Waveguide-Fed Magnetoelectric Dipole," *IEEE Antennas and Wireless Propagation Letters*, vol. 17, no. 8, pp. 1373-1376, Aug. 2018.

[7] K. Luk and B. Wu, "The Magnetoelectric Dipole—A Wideband Antenna for Base Stations in Mobile Communications," *Proceedings of the IEEE*, vol. 100, no. 7, pp. 2297-2307, July 2012.

[8] L. Ge and K. M. Luk, "A Magneto-Electric Dipole Antenna with Low-Profile and Simple Structure," *IEEE Antennas and Wireless Propagation Letters*, vol. 12, pp. 140-142, 2013.

[9] C. Ding and K. Luk, "Low-Profile Magneto-Electric Dipole Antenna," *IEEE Antennas and Wireless Propagation Letters*, vol. 15, pp. 1642-1644, 2016.

[10] M. Li, K. Luk, L. Ge and K. Zhang, "Miniaturization of Magnetoelectric Dipole Antenna by Using Metamaterial Loading," *IEEE Transactions on Antennas and Propagation*, vol. 64, no. 11, pp. 4914-4918, Nov. 2016.

[11] L. Siu, H. Wong and K. Luk, "A Dual-Polarized Magneto-Electric Dipole With Dielectric Loading," *IEEE Transactions on Antennas and Propagation*, vol. 57, no. 3, pp. 616-623, March 2009.

[12] Z. Zhang and K. Wu, "A Wideband Dual-Polarized Dielectric Magnetoelectric Dipole Antenna," *IEEE Transactions on Antennas and Propagation*, vol. 66, no. 10, pp. 5590-5595, Oct. 2018.

[13] J. Sun and K. Luk, "A Wideband Low Cost and Optically Transparent Water Patch Antenna with Omnidirectional Conical Beam Radiation Patterns," *IEEE Transactions on Antennas and Propagation*, vol. 65, no. 9, pp. 4478-4485, Sept. 2017.

[14] Z. Chen and H. Wong, "Liquid Dielectric Resonator Antenna with Circular Polarization Reconfigurability," *IEEE Transactions on Antennas and Propagation*, vol. 66, no. 1, pp. 444-449, Jan. 2018.

[15] L. Xing, Y. Huang, Y. Shen, S. Alja'afreh, Q. Xu, and R. Alrawashdeh, "Further investigation on water antennas," *IET Microwave, Antennas Propagation*, vol. 9, no. 8, pp. 735,-741, Jun. 2015.

[16] C. Hua and Z. Shen, "High-efficiency sea-water monopole antenna for maritime wireless communications," *IEEE Transactions on Antennas and Propagation*, vol. 62, no. 12, pp. 5968–5973, Dec. 2014.

[17] Z. Chen and H. Wong, "Wideband Glass and Liquid Cylindrical Dielectric Resonator Antenna for Pattern Reconfigurable Design," *IEEE Transactions on Antennas and Propagation*, vol. 65, no. 5, pp. 2157-2164, May 2017.

[18] C. Song, E. L. Bennett, J. Xiao, Q. Hua, L. Xing and Y. Huang, "Compact Ultra-Wideband Monopole Antennas Using Novel Liquid Loading Materials,*" IEEE Access*, vol. 7, pp. 49039-49047, Apr. 2019.

[19] C. Song, E. L. Bennett, J. Xiao, A. Alieldin, K. Luk and Y. Huang, "Metasurfaced, Broadband, and Circularly Polarized Liquid Antennas Using a Simple Structure," *IEEE Transactions on Antennas and Propagation*, vol. 67, no. 7, pp. 4907-4913, July 2019.

[20] C. Song, E. L. Bennett, J. Xiao, R. Pei, T. Jia, K. Luk and Y. Huang, "Passive beam-steering gravitational liquid antennas," *IEEE Transactions on Antennas and Propagation*, to be published, July 2019.

[21] E. L. Bennett, C. Song, Y. Huang and J. Xiao, "Measured Relative Complex Permittivities for Multiple Series of Ionic Liquids," *Journal of Molecular Liquids*, vol. 24, no. 11571, Nov. 2019

[22] X. Cui, F. Yang, M. Gao, L. Zhou, Z. Liang and F. Yan, "A Wideband Magnetoelectric Dipole Antenna with Microstrip Line Aperture-Coupled Excitation," *IEEE Transactions on Antennas and Propagation*, vol. 65, no. 12, pp. 7350-7354, Dec. 2017.

[23] K. M. Luk and K. W. Leung, *Dielectric Resonator Antennas*. Baldock, U.K.: Research Studies Press, 2003.

[24] M. Simeoni, R. Cicchetti, A. Yarovoy and D. Caratelli, "Plastic-Based Supershaped Dielectric Resonator Antennas for Wide-Band Applications," *IEEE Transactions on Antennas and Propagation*, vol. 59, no. 12, pp. 4820-4825, Dec. 2011.

[25] J. Zeng and K. Luk, "A Simple wideband magnetoelectric dipole antenna with a defected ground structure," *IEEE Antennas and Wireless Propagation Letters*, vol. 17, no. 8, pp. 1497-1500, Aug. 2018.

[26] K. Kang, Y. Shi and C. Liang, "Substrate integrated magneto–electric dipole for UWB application," *IEEE Antennas and Wireless Propagation Letters*, vol. 16, pp. 948-951, 2017.

[27] M. Li and K. Luk, "A differential-fed magneto-electric dipole antenna for UWB applications," *IEEE Transactions on Antennas and Propagation*, vol. 61, no. 1, pp. 92-99, Jan. 2013.

[28] L. Ge and K. M. Luk, "A magneto-electric dipole for unidirectional UWB communications," *IEEE Transactions on Antennas and Propagation*, vol. 61, no. 11, pp. 5762-5765, Nov. 2013.

[29] L. Ge and K. M. Luk, "A low-profile magneto-electric dipole antenna," *IEEE Transactions on Antennas and Propagation*, vol. 60, no. 4, pp. 1684-1689, Apr. 2012.

[30] J. Sun and K. Luk, "Wideband Linearly-Polarized and Circularly-Polarized Aperture-Coupled Magneto-Electric Dipole Antennas Fed by Microstrip Line with Electromagnetic Bandgap Surface," *IEEE Access*, vol. 7, pp. 43084-43091, 2019.

[31] F. Wu, and K.-M. Luk, "A Reconfigurable Magneto-Electric Dipole Antenna Using Bent Cross-Dipole Feed for Polarization Diversity," *IEEE Antennas Wireless Propag. Lett.*, vol. 16, pp. 412-415, 2017.

CHAOYUN SONG (M'16) received BEng. MSc and PhD degrees in electrical engineering and electronics from The University of Liverpool (UoL), Liverpool, UK, in 2012, 2013 and 2017, respectively.

He is currently an Assistant Professor with the School of Engineering and Physical Sciences (EPS), Heriot-Watt University, Edinburgh, Scotland, UK. He was a Postdoctoral Research Associate with UoL between 2017 and 2020. He has published more than 70 papers (including 30 IEEE transactions) in peer-reviewed journals and conference proceedings. He has held 2 US patents and 2 UK patents. His current research interests include wireless energy harvesting and wireless power transfer technologies, antennas and microwave circuits using novel materials, dielectric material and ionic liquids in RF applications, metamaterials and meta-surfaces in RF, energy harvesting and sensing technologies.

Dr. Song was the recipient of many international awards such as the BAE Systems Chairman's Award in 2017 for the innovation of next generation global navigation satellite system antennas. In 2018, he received the highly-commended award from the prestigious IET Innovation Awards over three categories – "Energy and Power", "Emerging Technologies" and "Young Innovators". Dr. Song has been a regular Reviewer of more than 25 international journals including Nature Communications, Applied Physics Letters, Nano Energy and seven IEEE transactions and a Guest Editor for Wireless Communications and Mobile Computing.
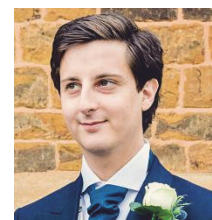
ELLIOT LEON BENNETT obtained his MChem and PhD degrees from Bangor University in 2009 and 2014 respectively, working across organic, inorganic and organometallic synthetic projects relating to various catalysts under Dr. M.A. Beckett and Dr. P.J. Murphy. He has also performed inelastic neutron scattering (INS) experiments at the ISIS neutron and muon source (Rutherford Appleton Laboratory) in collaboration with Dr. S.F. Parker and Dr. G.A. Chass. Dr. Bennett worked for 3 years in the group of Prof. G.G. Wildgoose as a senior postdoctoral research associate at the University of East Anglia (UEA) on energy applications of frustrated Lewis pair (FLP) chemistry, hydrogen activation using radical Lewis acids and the fundamental hydrogen activation mechanism of traditional FLP systems funded by the ERC PiHOMER Starting Grant. Currently Dr. Bennett works at the University of Liverpool (UoL) as a senior postdoctoral research associate under Prof. Xiao on ionic liquids, high permittivity solvents/organic molecules and dielectric materials for RF applications. Elliot has authored/coauthored more than 12 papers in international peer reviewed journals, patents and conference proceedings across the disciplines of metal-free & TM catalysis, organic/inorganic/organometallic synthesis, natural products, INS, FLP small molecule activation and liquid RF devices.
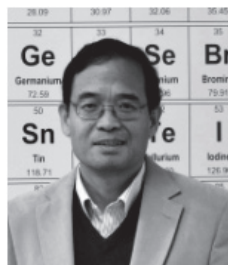
JIANLIANG XIAO received the B.Eng. at Northwest University in Xian in 1982. This was followed by an M.Eng. degree with Profs WU Chi and WANG Junyu at the RIPP in Beijing and a Ph.D. in chemistry at the University of Alberta under Prof Martin Cowie. After a postdoctoral appointment with Prof Richard Puddephatt, he joined the ERATO Catalysis Project directed by Prof Noyori. In 1996 he took up a Principal Scientist position at the University of Liverpool, becoming a Lecturer in 1999 and Professor in 2005 in the chemistry department. His research is concerned with the design, development and understanding of molecular catalysts for sustainable chemical synthesis, and he has published ca 200 papers in the area. He is a Changjiang Chair Professor and a Fellow of Royal Society of Chemistry.

YI HUANG (S'91 - M'96 - SM'06) received BSc in Physics (Wuhan University, China) in 1984, MSc (Eng) in Microwave Engineering (NRIET, Nanjing, China) in 1987, and DPhil in Communications from the University of Oxford, UK in 1994. He has been conducting research in the areas of wireless communications, applied electromagnetics, radar and antennas since 1987. His experience includes 3 years spent with NRIET (China) as a Radar Engineer and various periods with the Universities of Birmingham, Oxford, and Essex at the UK as a member of research staff. He worked as a Research Fellow at British Telecom Labs in 1994, and then joined the Department of Electrical Engineering & Electronics, the University of Liverpool, UK as a Faculty in 1995, where he is now a full Professor in Wireless Engineering, the Head of High Frequency Engineering Group and Deputy Head of Department. Prof. Huang has published over 350 refereed papers in leading international journals and conference proceedings, and authored Antennas: from Theory to Practice (John Wiley, 2008) and Reverberation Chambers: Theory and Applications to EMC and Antenna Measurements (John Wiley, 2016). He has received many research grants from research councils, government agencies, charity, EU and industry, acted as a consultant to various companies, and served on a number of national and international technical committees and been an Editor, Associate Editor or Guest Editor of five international journals. He has been a keynote/invited speaker and organiser of many conferences and workshops (e.g. WiCom 2006, 2010, IEEE iWAT2010, LAPC2012 and EuCAP2018). He is at present the Editor-in-Chief of Wireless Engineering and Technology, Associate Editor of IEEE Antennas and Wireless Propagation Letters, UK and Ireland Rep to European Association of Antenna and Propagation (EurAAP), a Senior Member of IEEE, a Fellow of IET, and Senior Fellow of HEA.